

Dual-Region Resonant Meander Metamaterial

Shridhar Manjunath, Mingkai Liu, Vidur Raj, Rifat A. Aoni, David A. Powell, Ilya V. Shadrivov, and Mohsen Rahmani*

Metamaterials are engineered structures designed to interact with electromagnetic radiation, whereby the frequency range in which metamaterials respond depends on their dimensions. In this paper, it is demonstrated that a metamaterial can be functional in more than one frequency region. An advanced metamaterial is demonstrated that can interact with both terahertz (THz) and near-infrared (NIR) frequencies, concurrently. This work exploits meander line resonators with nanoscale linewidth distributed over microscale areas, and experimentally demonstrates that such a metamaterial can simultaneously interact with NIR and THz waves. The engineered metamaterial acts as a plasmonic grating in the NIR range and simultaneously acts as an array of electric resonators in the THz range. Moreover, the performance of the engineered metamaterial is polarization-independent in both wavelength regions. Finally, a unique feature of the proposed metamaterial is that it enables resonant frequency tuning in the THz region without affecting the NIR response. All these novel advantages of dual-band meander metamaterial make it an ideal alternative for cutting-edge applications such as bi-functional sensing, imaging, filtering, modulation, and absorption.

an array of resonators, whereby the size of each meta-atom (unit cell) is generally a fraction of the operating wavelength.^[12] Hence, metamaterials can be approximated as homogenous media and effective medium theory is applied to calculate their electromagnetic responses.^[13] The meta-atom dimensions vary from millimeter to nanometer scales, corresponding to operation from microwaves to the visible frequency region, respectively.^[1–12] Metamaterials are distinct from photonic crystals and electromagnetic band-gap structures,^[14] due to their subwavelength unit cell size.

Metamaterials have been employed to realize many exotic properties and applications, such as sensing,^[6,15] reversed Doppler effect,^[2] negative refraction,^[16] cloaking,^[17,18] perfect lenses,^[19,20] absorbers,^[21] filters, polarizers,^[22–25] etc. However, to date, metamaterials have been largely designed to realize these applications in one frequency region only. For

instance, bio/chemical sensing via metamaterials is a popular technique for label-free detection,^[26,27] where the resonance frequency should be designed to match the unique absorption signature of the bio/chemical substance. While the spectral signatures of most organics, biomolecules, and explosives are in the terahertz (THz) region,^[28–33] many proteins and antibodies have analogous properties in the infrared range.^[34–36] However, a typical metamaterial can only target molecular fingerprints within a particular frequency range. Another example is where negative refraction is specific to a particular frequency region, i.e., THz, microwave, or near-infrared (NIR). Therefore, it would be of practical interest to have a single metamaterial that can support resonant responses at two or more spectral ranges that are far from each other. A number of works demonstrate dual or multi-band metamaterials,^[37–41] but the multiple bands are typically located at similar wavelength range. On the other hand, hybrid metamaterials consisting of metallic holes (functional at NIR) combined with cut wire structures (functional at THz) have been shown to be functional in both regions.^[42,43] However, each component is still functional in one frequency range only. To the best of our knowledge, there has been no demonstration to date of a single metamaterial with controlled interaction in dual spectral regions. Such a dual-region metamaterial can lead to the realization of many remarkable devices such as bio/chemical sensors, absorbers, and detectors, with dual functionality.

In this paper, we introduce and experimentally demonstrate a dual-region metamaterial which operates in two substantially


1. Introduction

Metamaterials are engineered subwavelength periodic structures, which exhibit unusual electromagnetic properties.^[1,2] Recent advances in fabrication techniques have enabled researchers to produce metamaterials working from radio waves to the visible frequency region.^[3–11] The optical properties of metamaterials are a result of the collective behavior of

S. Manjunath, Dr. M. Liu, R. A. Aoni, Prof. I. V. Shadrivov, Dr. M. Rahmani
Nonlinear Physics Centre
Research School of Physics
Australian National University
Canberra, ACT 2601, Australia
E-mail: Mohsen.rahmani@anu.edu.au

Dr. V. Raj
Department of Electronic Materials Engineering
Research School of Physics
Australian National University
Canberra, ACT 2601, Australia

Dr. D. A. Powell
School of Engineering and Information Technology
University of New South Wales Canberra
Canberra, ACT 2612, Australia

 The ORCID identification number(s) for the author(s) of this article can be found under <https://doi.org/10.1002/adom.201901658>.

DOI: 10.1002/adom.201901658

different frequency regimes. This novel platform paves the way toward dual-region photonics elements. Our metamaterial is realized by incorporating nanoscale features in a microscale design, whereby a meta-atom acts as a plasmonic grating in NIR and simultaneously acts as a highly subwavelength electric resonator at THz. Such a metamaterial structure requires precise tailoring of the electric field (E-field) response in both spectral regions. Therefore, the reduction of resonator feature size to the nanoscale is crucial. However, the geometries of metamaterials in the THz region are typically of micrometer scale, and discrete nanostructures do not interact strongly with THz waves. In our metamaterial, nanoscale features collectively form a microscale meta-atom which effectively interacts with THz wave.

Implementing nanoscale features can enable deeply subwavelength resonant structures with a high miniaturization factor at THz wavelengths. The miniaturization factor (λ_0/a) is defined as the ratio of the resonant wavelength (λ_0) to the length of the unit cell (a). Miniaturization allows metamaterials to be better described with effective medium theory by reducing complications from spatial dispersion.^[12,13,44] Meanwhile, miniaturization increases the number density of meta-atoms, allowing stronger light-matter interaction.^[45] A typical electrically excited THz resonator proposed by Chen et al. demonstrated a miniaturization factor of 5.7.^[45] However, the width of these resonator elements is several microns, therefore, NIR radiation would not interact with them. Alongside this, a few other designs have been proposed to miniaturize resonators, where they have obtained the miniaturization factor in the THz range of up to 15.5.^[45–50] However, these studies were aimed toward miniaturization alone, and did not investigate dual-region responses.

Here, we address the miniaturization issue by employing meander line resonators, which allow the implementation of nanoscale structures in the THz range. The meander line resonator is typically implemented as a deeply subwavelength microwave structure which is electrically excited in a polarization-dependent manner.^[46] Moreover, the unique design features of meander lines open up several applications, for example, a meander line design has been implemented as polarization converter, where a single layer of metamaterial converts an incident beam from one polarization to the other.^[51,52] Moreover, a meander structure with long strips of inductive lines is also ideal for absorbers due to its extremely dense packing of metal structures.^[53,54] Here, we downscale the dimensions of meander lines to the nanoscale. Such developments provide a unique opportunity to accommodate many lines in a small area. In this work, we take advantage of this property to design meander lines that are polarization-independent.

The optical response of a typical metamaterial depends on the polarization of the incident beam. Hence, realizing a polarization-independent metamaterial for dual-region applications is a challenging task, as it limits the orientation of inductor lines. Also, the angle of polarization affects the optical response of metamaterials, and subsequently any relevant applications. A polarization-independent structure would remove all the above complications. The reason for polarization-dependence is that typical metamaterials suffer from a lack of C_N ($N > 2$) symmetry.^[43] The current technique for producing symmetric meander lines with polarization-independence is to add multiple capacitors

along different polarization angles.^[49,50] However, this approach decreases the miniaturization factor. Here, by using nanoscale features, we eliminate the addition of capacitors along every polarization axis. This approach enables us to accommodate many nanoscale features without substantially affecting the resonant frequency. Nanoscale features decrease the size of the meta-atom significantly, so we can implement a supercell structure with C_4 symmetry and still obtain a very small lattice constant.

The major challenge to demonstrate dual-region polarization-independent metamaterial is fabricating a 5 mm by 5 mm area of nanostructured THz metamaterial. Such large area designs are generally fabricated by photolithographic techniques, which offer micrometer resolution at the best. Hence, THz resonators with nanoscale features cannot be achieved using traditional photolithography. Similar to meander resonators, there are a plethora of designs in the microwave region, which are several microns in width. However to realize these designs in THz region, the feature size must be reduced down to the nanoscale. Although electron-beam lithography (EBL) is widely used to fabricate nanoscale structures, it is not generally suitable for samples extending over a millimeter scale. In this work, we optimize EBL to fabricate THz samples with high speed and good accuracy. It enables us to fabricate inductor lines of 300 nm in width over 5 mm by 5 mm area. Therefore, such nanoscale inductive lines can resonate in the THz region and simultaneously act as a plasmonic grating at NIR.

Our dual-region metamaterial offers many potential applications as sensors, polarization manipulators, absorbers, wavefront controllers, etc. Sensing in the THz region is important as it can be used for chemical sensing,^[55,56] including detection of explosives and drugs,^[29,57] whereas NIR metamaterials are more commonly employed for biosensing.^[36] A dual-region metamaterial will enable both chemical sensing and biosensing with a single sensor. Alongside this, our proposed metamaterial allows controlling the light polarization and wave front shaping in THz and NIR, simultaneously. So far, such manipulations have been demonstrated either in NIR range^[52,58] or in THz region^[51,59] but not in both at the same time.

2. Structural Design

The design parameters are crucial to obtain a dual-region resonator as they define the frequency response in both regions (NIR and THz). The THz resonant frequency is defined as $\omega_0 = 1/\sqrt{LC}$, where L and C are the equivalent inductance and capacitance, respectively. A typical metamaterial resonator in THz is a 2D structure,^[45–50] where miniaturization is achieved by geometric scaling, i.e., increasing the capacitance or inductance without increasing the area occupied by the meta-atom. Hence, the degree of miniaturization is limited by geometrical parameters. Meander designs employ long and thin inductor lines with a small separation between the meta-atoms to decrease the resonant frequency. Therefore, employing meander designs can also lead to a high miniaturization ratio by increasing both inductance and capacitance.^[46] One of the highest reported miniaturization factors through meander design is proposed by Kolb et al.,^[46] where $\lambda_0/a = 31$ in the microwave region. But it is polarization-dependent and operational only in the microwave region.

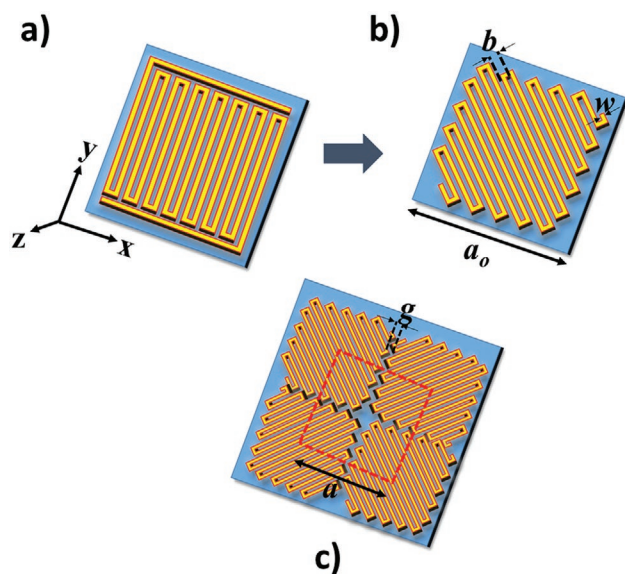


Figure 1. a) Polarization-dependent meander line resonator in microwave region^[46] and b) Proposed meander line resonator design in THz region, with parameters w (width of meander) = 300 nm, b (period of meander) = 1 μm , a_0 (length of unit cell) = 16.26 μm . The thickness of the metal layer is 200 nm. c) A supercell with fourfold symmetry that produces polarization-independence property, where $g = 500$ nm is the gap between unit cells and $a = 23$ μm is the lattice constant (as indicated in the red box).

To design a dual-region polarization-independent resonator, several factors have been taken into account. First we have eliminated the polarization-dependence of the meander lines. To this end, we have employed a symmetric resonator to couple with incident waves equally for both transverse electric and transverse magnetic polarizations. Subsequently, we have optimized THz and finally NIR resonant frequencies. A typical meander resonator shown in **Figure 1a** lacks symmetrical distribution of meander lines along x and y axis, causing a difference in the optical response. Hence, we initially arrange meander lines at 45° (C_2 symmetry) as shown in **Figure 1b**, where the structure is symmetric along x and y axis. This leads to the same frequency response along both x and y polarization directions, but fails for skewed (x/y axis) polarization angles. To obtain polarization-independence with a C_2 symmetric structure, we implement C_4 symmetry,^[60] whereby each alternating meta-atoms are rotated by 90° (see **Figure 1c**). This configuration results in a supercell structure with four individual meta-atoms which leads to the same optical response for all the polarization angles. Each supercell is overlapped with adjacent supercells to form a single metamaterial surface. Accordingly, the length of meta-atom changes to lattice constant a (which is $\sqrt{2}$ times a_0 as indicated by the red box in **Figure 1c**).

As our THz experimental apparatus has maximum signal to noise ratio at around 0.6 THz, we designed our metamaterial to be resonant at this frequency. The proposed design is shown in **Figure 1c**, where the width and the period of meander lines are $w = 300$ nm, and $b = 1$ μm , respectively. Meanwhile, the spacing between the meta-atoms is $g = 500$ nm and the lattice constant $a = 23$ μm . We chose gold and quartz as the materials for the

metamaterial and the substrate, respectively. We simulated the response of the metamaterials at 0.3–1.1 THz using CST microwave studio, as a unit cell with periodic boundary conditions. The permittivity of the quartz substrate is taken as 3.83 with no losses.^[61] A Drude model was used for the gold layer, with a collision frequency of 4.07×10^{13} rad s^{-1} and a plasma frequency of 1.37×10^{16} rad s^{-1} .^[62,63] **Figure 2** shows the

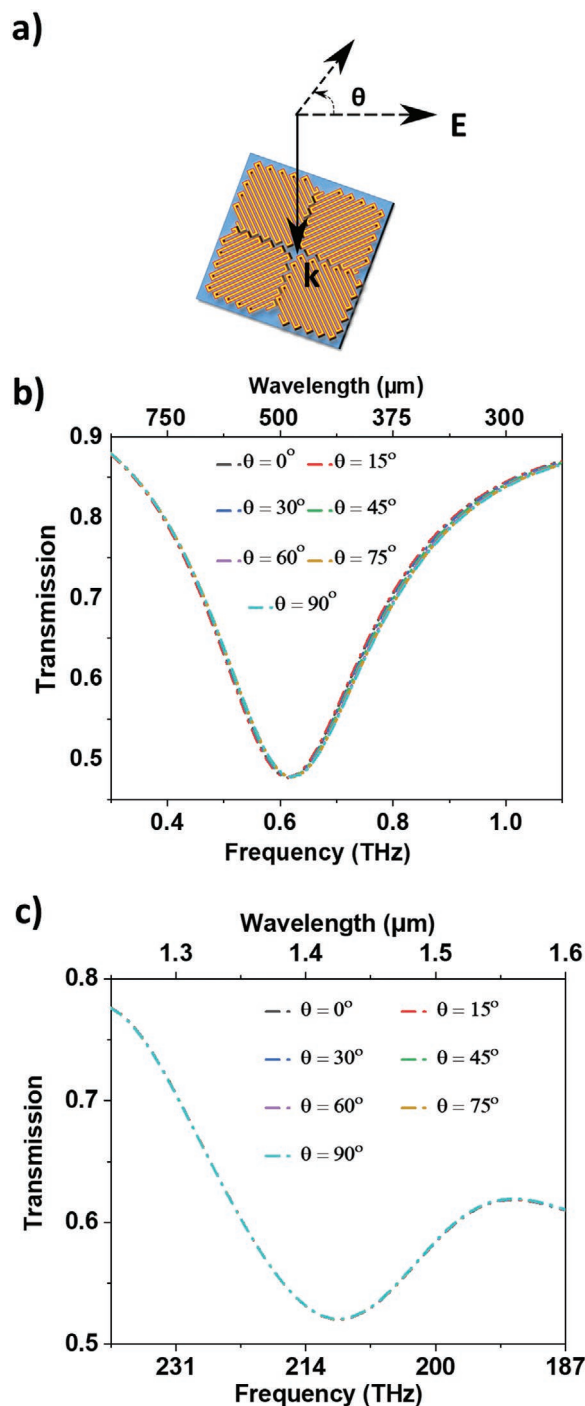


Figure 2. a) Schematic for the incident polarization angle. Resonant transmission response of proposed design in b) the THz and c) near-infrared (NIR) regions for various angles of polarization excitation.

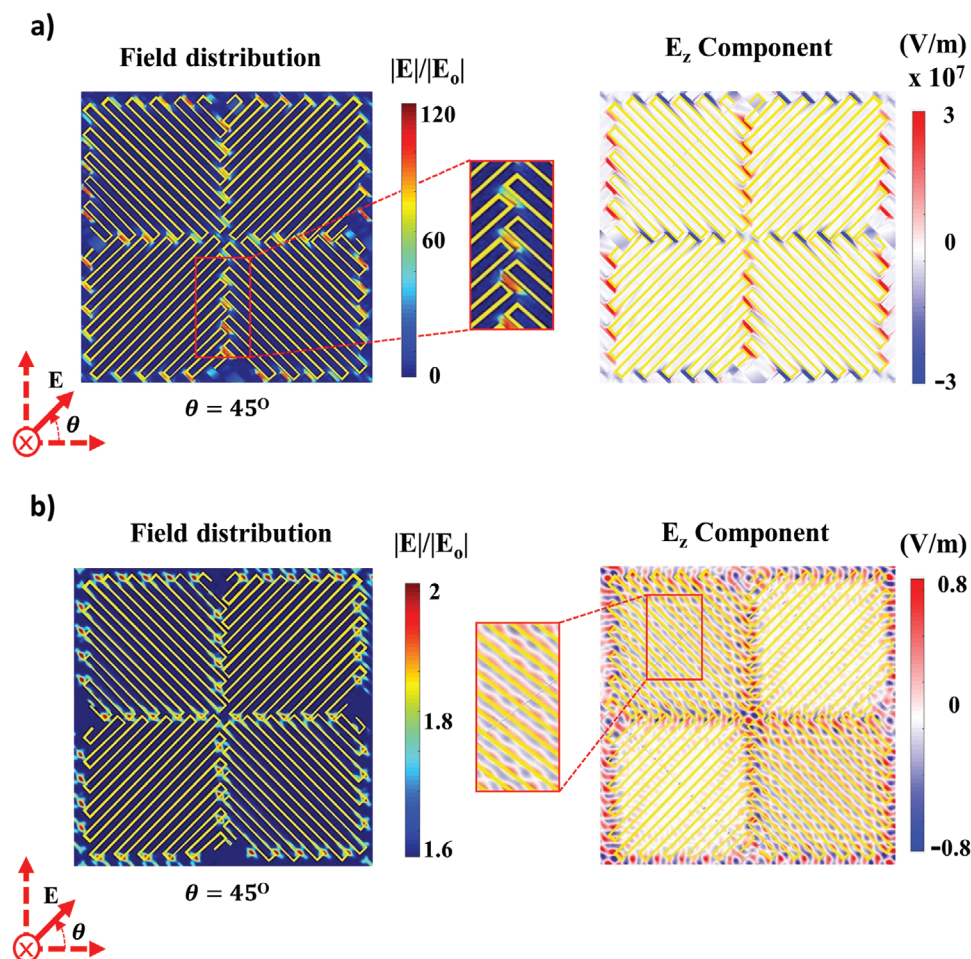


Figure 3. Left panels represent normalized near field distribution on the surface of the unit cells, and right panels represent E_z (electric-field along propagation of the incident wave) component on the surface of the unit cells, simulated at a) 0.62 THz and b) 212 THz ($1.42 \mu\text{m}$).

numerically simulated transmission spectra of our designed metamaterial. Figure 2a illustrates the configuration of the metamaterial and the incident wave, where θ is the angle of polarization. Figure 2b shows that the optimized meta-atom exhibits a transmission dip at 0.62 THz for all polarization angles, corresponding to a miniaturization ratio (λ_0/a) of 21.03.

The THz resonance mainly arises from the electric dipole moment of the very long meander lines, particularly the strong electric field in the gaps between them. The meander lines form a microscale meta-atom in the THz region, acting as a very long inductor, with the gaps in between acting as a capacitor, to give a series LC response. The scenario is different in the NIR range, where the wavelength is comparable to the width of meander lines. When the meander lines are excited with a shorter wavelength (NIR), each meta-atom acts like a plasmonic grating. The nanoscale features with period b , produce grating resonances in the NIR. The lattice constant of the meta-atom is $23 \mu\text{m}$, which is extremely large for a NIR metamaterial structure. As it is challenging to simulate large structures with very fine mesh using CST microwave studio, we have used finite difference time domain Lumerical software for modeling the electromagnetic responses in the NIR region.

The simulations illustrate a resonant frequency at 212 THz, ($\sim 1.42 \mu\text{m}$) (see Figure 2c). This resonance is also independent of polarization due to the C_4 symmetry of the structure, as shown by the overlap of all curves in Figure 2c. Indeed, our engineered meander resonator with nanoscale features not only produces dual-region resonances in NIR and THz simultaneously, but also removes the polarization-dependence in both of these regions.

To get a better understanding of the physics behind this metamaterial, we have simulated the near field distribution on the surface of meta-atoms (see Figure 3) at the resonant frequencies of 0.62 THz and 212 THz ($\approx 1.42 \mu\text{m}$). In the THz region, the resonance frequency depends upon the total length of meander line, the internal period of the meander line b , and the gap g between each meta-atom. As shown in Figure 3, the left panels represent the near-field distribution. For both frequency regions the electric field strength is very high at the gaps between meta-atoms. The right panels represent the distribution of charges (E_z component). Figure 3a (both panels) shows, for the THz case, the interaction between individual meander lines is very weak compared to the external interaction in the gaps between meta-atoms. Since the meander

lines are short compared to the wavelength, the charges on each side of the gap are essentially in phase, and the contribution of the internal capacitance is negligible compared to the external capacitance. The choice of C_4 symmetry enables us to extend the meta-atom inside the bounding box of its neighbors, thereby increasing the interaction. However, this scenario is different in the NIR, where each meander line no longer acts as a single inductor, but effectively becomes a series of grating lines. Figure 3b (left panel) shows the field enhancement at the NIR resonance is one order of magnitude lower than at the THz resonance.

It is worth noting that, the length of each inductor line is equivalent to several NIR wavelengths. The grating behavior can be observed by the E_z component as shown in Figure 3b, right panel. Meander lines which are perpendicular to the E-field act as a plasmonic grating, leading to interactions between individual lines. In contrast, when the E-field is parallel to the grating lines, the incident wave does not couple with meander lines at this wavelength. Figure 3 contains one more message: the strong E-field enhancement at the gaps between meta-atoms indicates that the THz resonant frequency is highly sensitive to the gap (g), while the grating resonance in NIR depends on the period of the meander lines (b). This property demonstrates that each of the frequency regions can be tuned independently.

The optical properties of metamaterials are in general highly dependent on the wavelength. Very often, for practical applications of metamaterials, the resonance frequencies have to be tuned to the desired wavelength to match the spectral signatures of analytes. In our proposed design, the number of inductor lines is 21 and any variation to this number affects the optical response of the metamaterial in both NIR and THz regions. Alongside this, the exact values of inductance and capacitance cannot be determined by the length of the line meander alone, as they depend on the spacing between each line.^[46] However, the THz resonant frequency can be tuned to the desired frequency easily by increasing the gap g between meta-atoms, while this variation does not affect the NIR resonance. **Figure 4** shows varying g tunes the THz resonant frequency, while having negligible influence on the NIR resonant frequency. This allows the resonance to be precisely positioned both frequency regimes. In Figure 4a, the gap g is varied from 200 to 800 nm, and the THz resonant frequency changes from 0.5 to 0.7 THz, while in Figure 4b the NIR resonance remains at 1.42 μm . This means that our proposed design has more freedom to control the resonant frequency in both regions as compared to typical resonators (see Supporting Information).

3. Experimental Verification

To verify the proposed structure, it was fabricated using EBL. To increase the speed of the electron beam writing considerably, a 10 μm aperture size of the electron beam and a 20 nm step size of a 30 kV Raith 150 tool were employed. Optimizing the above-mentioned parameters increased the writing speed without affecting resolution, so patterning of 5 mm \times 5 mm area could be achieved in a few hours.

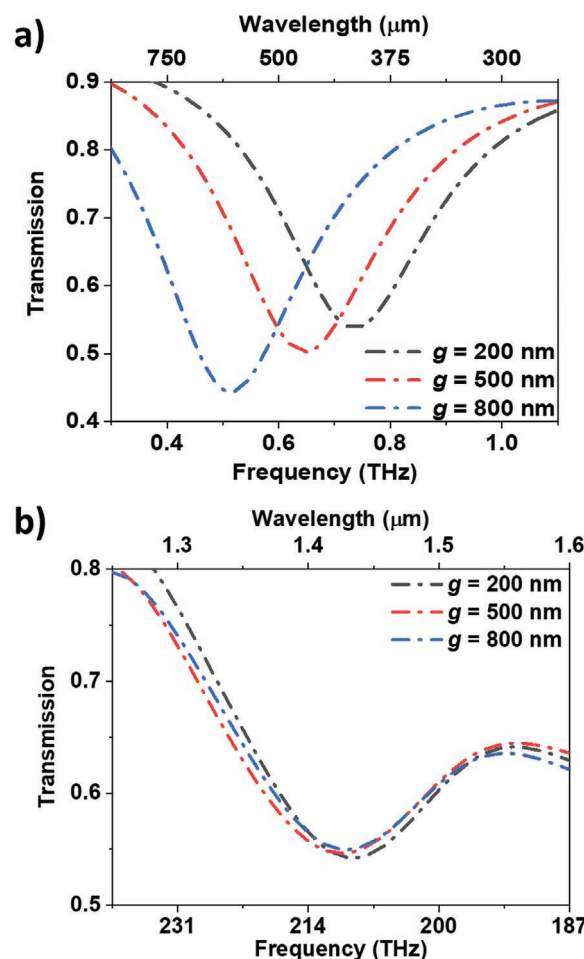


Figure 4. Simulated transmission response showing a) resonant frequency tuning in THz, and b) resonant frequency at near-infrared by changing the value of g .

An optical microscopy image of the metamaterial can be seen in **Figure 5a**. NIR and THz measurements were performed using separate experimental apparatus. The transmission spectra in the THz region were measured by THz time-domain spectroscopy (THz-TDS), and are shown in **Figure 5b**. As can be seen, there is a very good agreement between the predicted spectra in **Figure 2b** and the experimental measurements in **Figure 5b**. The discrepancy in resonant frequency between simulation and experimental results was due to the fabrication imperfections. Given the large area on which the nanoscale structures were fabricated, some non-uniformities were expected to take place across the sample. Moreover, nanoscale features and the surface roughness also increased the effective ohmic losses in the meander lines, causing higher absorption in the gold layer that was neglected in the simulations.^[59] These issues could affect the overall optical properties of the sample.

The transmission spectrum was measured along different polarization axes, confirming the polarization-independent behavior expected for a structure with C_4 symmetry. However, the miniaturization factor reduced to 18.63 due to the slight shift in resonant frequency, nevertheless this is the

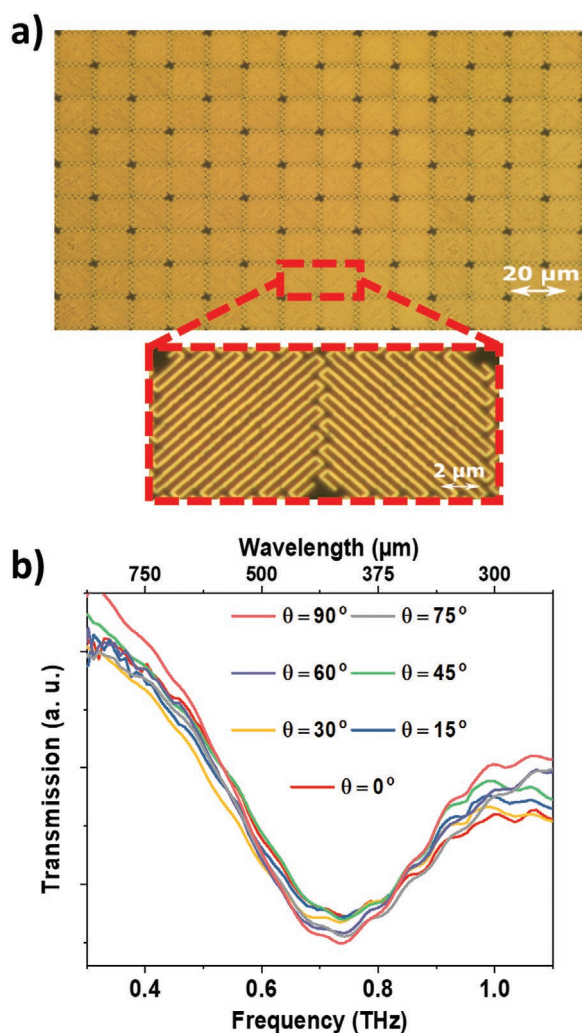


Figure 5. a) Optical microscopy images of the fabricated design. b) Experimental results of resonant frequency response for different polarization angles in the THz range.

highest miniaturization factor achieved for polarization-independent THz metamaterial resonator.^[45–50,64–73] It is worth mentioning that in this design the Q factor was mainly affected by the density of the unit cells. As discussed in ref. [45], the Q factor decreased with the increase in the density of the cells. The NIR frequency response was measured using a homemade spectroscopy set-up, where the sample was uniformly illuminated with a broadband white light source. **Figure 6a** shows the scanning electron microscopy (SEM) image of the metamaterial. The transmission spectra for the aforementioned design parameters are presented in **Figure 6b**. The resonance can be observed at the wavelength of 1.4 μm . Similarly, the experiment was repeated by varying the polarization axis of the incident light in steps of 15°. The resonant frequency response for every polarization angle closely resembled the theoretical predictions (see **Figures 2c** and **6b**), which confirmed the polarization-independence of the resonant response at NIR.

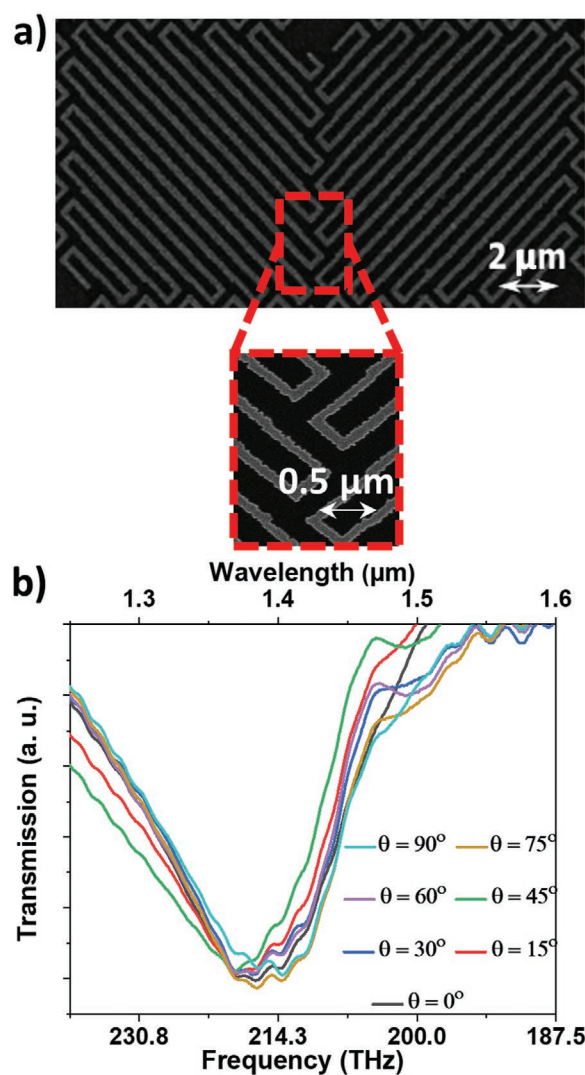


Figure 6. a) Scanning electron microscopy (SEM) images of the proposed design. b) Experimental verification of resonant frequency response for different polarization angles in the near-infrared region.

4. Conclusion

In summary, we have demonstrated a single metamaterial resonator with dual-region resonant responses at THz and NIR frequencies. We have designed and fabricated a meander line metamaterial at the nanoscale, realizing a deep subwavelength THz metamaterial resonator (miniaturization factor $\lambda_0/a = 18.63$) and simultaneously a NIR plasmonic grating. Moreover, our metamaterial is designed with C_4 symmetry that ensures polarization-independent responses in both wavelength regions. Another unique feature of our design is that its resonance in the THz region can be tuned without affecting the optical properties at NIR, because the resonances at THz and NIR frequencies are sensitive to different geometrical parameters. Our design opens up the prospect for dual-region applications in bio/chemical sensing, detectors, and absorbers.

Supporting Information

Supporting Information is available from the Wiley Online Library or from the author.

Acknowledgements

S.M. and M.L. contributed equally to this work. The Australian Research Council is acknowledged for its financial support. The fabrication of the samples was performed at the Australian National Fabrication Facility, ACT node. The authors thank Neil Mansfield at Nottingham Trent University for helpful discussions. We acknowledge the support of Our Health in Our Hands, a strategic initiative of the Australian National University, which aims to transform healthcare by developing new personalised health technologies and solutions in collaboration with patients, clinicians, and health care providers.

Conflict of Interest

The authors declare no conflict of interest.

Keywords

dual-region, meander metamaterial, polarization-independence

Received: October 4, 2019

Revised: December 17, 2019

Published online: February 19, 2020

- [1] D. R. Smith, W. J. Padilla, D. C. Vier, S. C. Nemat-Nasser, S. Schultz, *Phys. Rev. Lett.* **2000**, *84*, 4184.
- [2] V. G. Vesalago, *Phys. -Usp.* **1968**, *10*, 509.
- [3] M. C. K. Wiltshire, J. B. Pendry, I. R. Young, D. J. Larkman, D. J. Gilderdale, J. V. Hajnal, *Science* **2001**, *291*, 849.
- [4] I. Shadrivov, S. K. Morrison, Y. S. Kivshar, *Opt. Express* **2006**, *14*, 9344.
- [5] H. Chen, W. J. Padilla, J. M. O. Zide, A. C. Gossard, A. J. Taylor, R. D. Averitt, *Nature* **2006**, *444*, 597.
- [6] C. Zaichun, M. Rahmani, G. Yandong, C. T. Chong, H. Minghui, *Adv. Mater.* **2012**, *24*, OP143.
- [7] S. Zhang, W. Fan, N. C. Panoiu, K. J. Malloy, R. M. Osgood, S. R. J. Brueck, *Phys. Rev. Lett.* **2005**, *95*, 137404.
- [8] I. Staude, A. E. Miroshnichenko, M. Decker, N. T. Fofang, S. Liu, E. Gonzales, J. Dominguez, T. S. Luk, D. N. Neshev, I. Brener, Y. S. Kivshar, *ACS Nano* **2013**, *7*, 7824.
- [9] M. Rahmani, L. Xu, A. E. Miroshnichenko, A. Komar, R. C. Morales, H. Chen, Y. Zarate, S. Kruk, G. Zhang, D. N. Neshev, Y. S. Kivshar, *Adv. Funct. Mater.* **2017**, *27*, 1700580.
- [10] K. Z. Kamali, L. Xu, J. Ward, K. Wang, G. Li, A. E. Miroshnichenko, D. Neshev, M. Rahmani, *Small* **2019**, *15*, 1805142.
- [11] M. Rahmani, G. Leo, I. Brener, A. V. Zayats, S. A. Maier, C. D. Angelis, H. Tan, V. F. Gili, F. Karouta, R. Oulton, K. Vora, M. Lysevych, I. Staude, L. Xu, A. E. Miroshnichenko, C. Jagadish, D. N. Neshev, *Opto-Electron. Adv.* **2018**, *1*, 18002101.
- [12] C. Caloz, A. Lai, T. Itoh, *New J. Phys.* **2005**, *7*, 167.
- [13] N. I. Landy, C. M. Bingham, T. Tyler, N. Jokerst, D. R. Smith, W. J. Padilla, *Phys. Rev. B* **2009**, *79*, 125104.
- [14] R. Liu, T. J. Cui, D. Huang, B. Zhao, D. R. Smith, *Phys. Rev. E* **2007**, *76*, 026606.
- [15] J. F. O'Hara, R. Singh, I. Brener, E. Smirnova, J. Han, A. J. Taylor, W. Zhang, *Opt. Express* **2008**, *16*, 1786.
- [16] R. A. Shelby, D. R. Smith, S. Schultz, *Science* **2001**, *292*, 77.
- [17] W. Cai, U. K. Chettiar, A. V. Kildishev, V. M. Shalev, *Nat. Photonics* **2007**, *1*, 224.
- [18] D. Schurig, J. J. Mock, B. J. Justice, S. A. Cummer, J. B. Pendry, A. F. Starr, D. R. Smith, *Science* **2006**, *314*, 977.
- [19] J. B. Pendry, *Phys. Rev. Lett.* **2000**, *85*, 3966.
- [20] N. Yu, F. Capasso, *Nat. Mater.* **2014**, *13*, 139.
- [21] N. Liu, M. Mesch, T. Weiss, M. Hentschel, H. Giessen, *Nano Lett.* **2010**, *10*, 2342.
- [22] D. A. Powell, M. Lapine, M. V. Gorkunov, I. V. Shadrivov, Y. S. Kivshar, *Phys. Rev. B* **2010**, *82*, 155128.
- [23] M. Liu, D. A. Powell, R. Guo, I. V. Shadrivov, Y. S. Kivshar, *Adv. Opt. Mater.* **2017**, *5*, 1600760.
- [24] Y. Zhao, M. A. Belkin, A. Alu, *Nat. Commun.* **2012**, *3*, 870.
- [25] A. Vakil, N. Engheta, *Science* **2011**, *332*, 1291.
- [26] H. Yoshida, Y. Ogawa, Y. Kawai, *Appl. Phys. Lett.* **2007**, *91*, 253901.
- [27] A. V. Kabashin, P. Evans, S. Pastkovsky, W. Hendren, G. A. Wurtz, R. Atkinson, R. Pollard, V. A. Podolskiy, A. V. Zayats, *Nat. Mater.* **2009**, *8*, 867.
- [28] D. Lee, J. Kang, J. Kwon, J. Lee, S. Lee, D. Woo, J. H. Kim, C. Song, Q. Park, M. Seo, *Sci. Rep.* **2017**, *7*, 8146.
- [29] J. Chen, Y. Chen, H. Zhao, G. J. Bastiaans, X. C. Zhang, *Opt. Express* **2007**, *15*, 12060.
- [30] Y. Zhang, T. Li, B. Zeng, H. Zhang, H. Lv, X. Huang, W. Zhang, A. K. Azad, *Nanoscale* **2015**, *7*, 12682.
- [31] R. Liu, M. He, R. Su, Y. Yu, W. Qi, Z. He, *Biochem. Biophys. Res. Commun.* **2010**, *391*, 862.
- [32] Z. Geng, X. Zhang, Z. Fan, X. Lv, H. Chen, *Sci. Rep.* **2017**, *7*, 16378.
- [33] B. M. Fischer, M. Walther, P. U. Jepsen, *Phys. Med. Biol.* **2002**, *47*, 3807.
- [34] M. A. Ochsenkuhn, C. J. Campbell, *Chem. Commun.* **2010**, *46*, 2799.
- [35] C. Wu, A. B. Khanikaev, R. Adato, N. Arju, A. A. Yanik, H. Altug, G. Shvets, *Nat. Mater.* **2012**, *11*, 69.
- [36] A. Tittl, A. Leitis, M. Liu, F. Yesilkoy, D. Y. Choi, D. N. Neshev, Y. S. Kivshar, H. Altug, *Science* **2018**, *360*, 1105.
- [37] Z. H. Jiang, S. Yun, F. Toor, D. H. Werner, T. S. Mayer, *ACS Nano* **2011**, *5*, 4641.
- [38] Y. Ma, Q. Chen, J. Grant, S. C. Saha, A. Khalid, D. R. S. Cumming, *Opt. Lett.* **2011**, *36*, 945.
- [39] H. Tao, C. M. Bingham, D. Pilon, K. Fan, A. C. Strikwerda, D. Shrekenhamer, W. J. Padilla, X. Zhang, R. D. Averitt, *J. Phys. D: Appl. Phys.* **2010**, *43*, 225102.
- [40] X. Shen, T. J. Cui, J. Zhao, H. F. Ma, W. X. Jiang, H. Li, *Opt. Express* **2011**, *19*, 9401.
- [41] H. Li, L. H. Yuan, B. Zhou, X. P. Shen, Q. Cheng, T. J. Cui, *J. Appl. Phys.* **2011**, *110*, 014909.
- [42] I. J. H. McCrindle, J. P. Grant, L. C. P. Gouveia, D. R. S. Cumming, *Phys. Status Solidi A* **2015**, *212*, 1625.
- [43] J. Grant, I. J. H. McCrindle, D. R. S. Cumming, *Opt. Express* **2016**, *24*, 3451.
- [44] J. B. Pendry, A. J. Holden, D. J. Robbins, W. J. Stewart, *IEEE Trans. Microwave Theory Tech.* **1999**, *47*, 2075.
- [45] R. Singh, C. Rockstuhl, W. Zhang, *Appl. Phys. Lett.* **2010**, *97*, 241108.
- [46] P. W. Kolb, T. S. Salter, J. A. McGee, H. D. Drew, W. J. Padilla, *J. Appl. Phys.* **2011**, *110*, 054906.
- [47] W. J. Padilla, M. T. Aronsson, C. Highstrete, M. Lee, A. J. Taylor, R. D. Averitt, *Phys. Rev. B* **2007**, *75*, 041102.
- [48] X. Zhang, Q. Li, W. Cao, J. Gu, R. Singh, Z. Tian, J. Han, W. Zhang, *IEEE J. Sel. Top. Quantum Electron.* **2013**, *19*, 8400707.
- [49] Y. Chen, H. Zhou, X. Tan, S. Jiang, A. Yang, J. Li, M. Hou, Q. Guo, S. W. Wang, F. Liu, H. Liu, F. Yi, *IEEE Photonics J.* **2018**, *10*, 4600409.
- [50] I. A. I. Al-Naib, C. Jansen, N. Born, M. Koch, *Appl. Phys. Lett.* **2011**, *98*, 091107.

- [51] P. Fei, Z. Shen, X. Wen, F. Nian, *IEEE Trans. Antennas Propag.* **2015**, 63, 4609.
- [52] Y. Cheng, C. Fang, X. S. Mao, R. Z. Gong, L. Wu, *IEEE Photonics J.* **2016**, 8, 7805509.
- [53] N. Bai, Y. Liu, C. Shen, X. Sun, *IEEE Trans. Electron Devices* **2017**, 64, 2949.
- [54] Y. Cheng, Y. Zou, H. Luo, F. Chen, X. Mao, *J. Electron. Mater.* **2019**, 48, 3969.
- [55] J. Li, Z. Tian, Y. Chen, W. Cao, Z. Zeng, *Appl. Opt.* **2012**, 51, 3258.
- [56] K. Kawase, Y. Ogawa, Y. Watanabe, *Opt. Express* **2003**, 11, 2549.
- [57] J. F. Federici, B. Schulkin, F. Huang, D. Gary, R. Barat, F. Oliveira, D. Zimdars, *Semicond. Sci. Technol.* **2005**, 20, S266.
- [58] C. Chu, M. L. Tseng, J. Chen, P. C. Wu, Y. Chen, H. Wang, T. Chen, W. T. Hsieh, H. J. Wu, G. Sun, D. P. Tsai, *Laser Photonics Rev.* **2016**, 10, 1600106.
- [59] M. Liu, Q. Yang, A. R. Rifat, V. Raj, A. Komar, J. Han, M. Rahmani, H. T. Hattori, D. Neshev, D. A. Powell, I. V. Shadrivov, *Adv. Opt. Mater.* **2019**, 7, 1900736.
- [60] C. Menzel, C. Rockstuhl, F. Lederer, *Phys. Rev. A* **2010**, 82, 053811.
- [61] M. Naftaly, R. E. Miles, *Proc. IEEE* **2007**, 95, 1658.
- [62] M. A. Ordal, L. L. Long, R. J. Bell, S. E. Bell, R. R. Bell, R. W. Alexander Jr., C. A. Ward, *Appl. Opt.* **1983**, 22, 1099.
- [63] M. Walter, D. G. Cooke, C. Sherstan, M. Hajar, M. R. Freeman, F. A. Hegmann, *Phys. Rev. B* **2007**, 76, 125408.
- [64] W. Withayachumnankul, C. Fumeaux, D. Abbott, *Opt. Express* **2010**, 18, 25912.
- [65] H. T. Chen, J. F. O'Hara, A. J. Taylor, R. D. Averitt, *Opt. Express* **2007**, 15, 1084.
- [66] T. D. Karamanos, N. V. Kantartzis, *Proc. SPIE* **2014**, 9125, 912511.
- [67] D. Schurig, J. J. Mock, D. R. Smith, *Appl. Phys. Lett.* **2006**, 88, 041109.
- [68] M. Chen, L. Singh, N. Xu, R. Singh, W. Zhang, L. Xie, *Opt. Express* **2017**, 25, 14089.
- [69] S. Wang, L. Xia, H. Mao, X. Jiang, S. Yan, H. Wang, D. Wei, H. L. Cui, C. Du, *IEEE Photonics Technol. Lett.* **2016**, 28, 986.
- [70] Y. Cheng, H. Zou, J. Yang, X. Mao, R. Gong, *Opt. Mater. Express* **2018**, 8, 3104.
- [71] D. Y. Shchegolkov, A. K. Azad, J. F. O'Hara, E. I. Simakov, *Phys. Rev. B* **2010**, 82, 205117.
- [72] D. R. Chowdhury, R. Singh, M. Reiten, H. T. Chen, A. J. Taylor, J. F. O'Hara, A. K. Azad, *Opt. Express* **2011**, 19, 15817.
- [73] J. Li, C. M. Shah, W. Withayachumnankul, B. S. Y. Ung, A. Mitchell, S. Sriram, M. Bhaskaran, S. Chang, D. Abbott, *Opt. Lett.* **2013**, 38, 2104.